

## Chapter 5

# Relativistic Cyclotron

**Abstract** This chapter introduces to the AVF (azimuthally varying field), isochronous, relativistic cyclotron, and to the theoretical material needed for the simulation exercises. A brief reminder of the historical context is followed by further basic theoretical considerations leaning on the cyclotron concepts introduced in Chapter 4 and including

- Thomas focusing and the AVF cyclotron,
- positive focusing index,
- isochronous optics,
- separated sector cyclotrons,
- spin dynamics in an AVF cyclotron.

Simulation exercises use optical elements and keywords met earlier: the analytical field modeling DIPOLE, TOSCA in case using a field map is preferred, CAVITE to accelerate, SPNTRK to solve spin motion, FAISCEAU, FAISTORE, FIT, etc. The exercises further develop on radial and spiral sector magnets, edge focusing and flutter, isochronous optics, separated sector ring cyclotrons, and their modeling as part of DIPOLE, DIPOLES and other CYCLOTRON keyword capabilities.

## 1474 Notations used in the Text

$B; B_0$	field value; at reference radius $R_0$
$\mathbf{B}; B_R; B_\theta; B_y$	field vector; radial, azimuthal and axial components
$BR = p/q; BR_0$	magnetic rigidity; reference rigidity
$C; C_0$	orbit length, $C = 2\pi R$ ; reference, $C_0 = 2\pi R_0$
$E$	ion energy
EFB	effective Field Boundary
$\mathcal{F}, F$	azimuthal field form factor; flutter, $F = \left( \frac{\langle (\mathcal{F} - \langle \mathcal{F} \rangle)^2 \rangle}{\langle \mathcal{F} \rangle^2} \right)^{1/2}$
$f_{\text{rev}}, f_{\text{rf}}$	revolution and accelerating voltage frequencies
$h$	harmonic number, an integer, $h = f_{\text{rf}}/f_{\text{rev}}$
$k = \frac{R}{B} \frac{dB}{dR}$	geometric index, a global quantity
$n = \frac{\rho}{B} \frac{dB}{d\rho}$	focusing index, a local quantity
$m; m_0; M$	mass; rest mass; in units of $\text{MeV}/c^2$
$\mathbf{p}; p_0$	ion momentum vector; reference momentum
$q$	ion charge
$R, R_0, R_E$	average orbital radius, $R = C/2\pi$ ; $R(p = p_0)$ ; $R(E)$
$\mathcal{R}$	radial field form factor
1475 $RF$	Radio-Frequency: as per the accelerating voltage technology
$s$	path variable
$T_{\text{rev}}, T_{\text{rf}}$	revolution and accelerating voltage periods
$v$	ion velocity
$V(t); \hat{V}$	oscillating voltage; its peak value
$x, x', y, y'$	radial and axial coordinates in moving frame $[(*)' = d(*)/ds]$
$\alpha$	momentum compaction
$\alpha$	trajectory deviation
$\beta = v/c; \beta_0; \beta_s$	normalized ion velocity; reference; synchronous
$\gamma = E/m_0$	Lorentz relativistic factor
$\Delta p, \delta p$	momentum offset
$\varepsilon$	wedge angle
$\epsilon_R$	strength of a depolarizing resonance
$\varepsilon_u$	Courant-Snyder invariant ( $u : x, y, l, \dots$ )
$\zeta$	spiral angle of a spiral sector dipole EFB
$\theta$	azimuthal angle
$\phi; \phi_s$	phase of oscillating voltage; synchronous phase

## 1476 5.1 Introduction

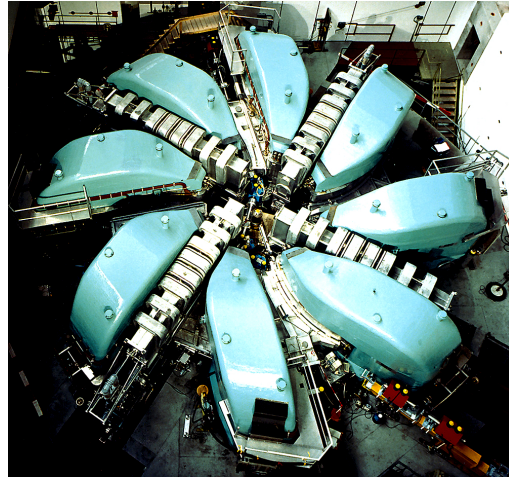
1477 Isochronous cyclotrons are in operation today by the thousands, tens are produced  
 1478 each year, applications include production of radio-isotopes mostly; proton therapy  
 1479 (Fig. 5.1), a rapidly growing field; high power beams and secondary particle beam

1480 production (Fig. 5.2). Cryogeny and high fields further allow compactness (Fig. 5.1)  
 1481 as well as highest rigidity (Fig. 5.3)

**Fig. 5.1** COMET proton-therapy cyclotron at PSI. A 250 MeV, 500 nA, 4-sector isochronous AVF cyclotron, the spiral poles enhance axial focusing. A 3 m diameter superconducting coil provides the dipole field [1]

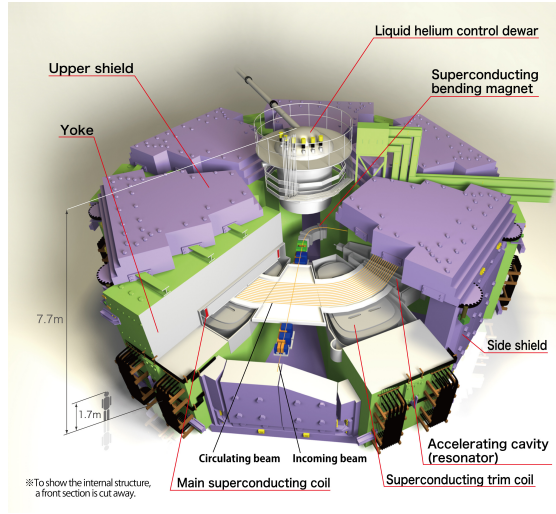


**Fig. 5.2** PSI 590 MeV ring cyclotron delivers a 1.4 MW proton beam. Acceleration takes  $\sim 180$  turns; extraction efficiency is  $> 99.99\%$ ; overall diameter is 15 m. Beam is used for the production of secondary neutron and muon beams [2]



1482 At the origin of the evolution towards the AVF cyclotron in the late 1930s is  
 1483 the energy limitation, at a few 10s of MeV, of the classical cyclotron technology  
 1484 (Chap. 4). Axial focusing in the latter is obtained by a slow decrease of the guiding  
 1485 field with radius: a negative index  $-1 < k < 0$ , resulting in both radial and axial  
 1486 periodic stability (Eq. 4.16). Isochronism requires instead the field to increase with

**Fig. 5.3** RIKEN K2500, superconducting coil, separated-sector ring cyclotron [3]. The dipole field is 3.8 T, rigidity 8 T m, diameter 18.4 m, 8,300 ton. Beam injection radius is 3.56 m, extraction radius is 5.36 m. The cyclotron is part of a heavy-ion accelerator complex [4]



radius, field index  $k > 0$ , a consequence of  $B(R) \propto \gamma(R)$  (Sect. 5.2). The AVF concept

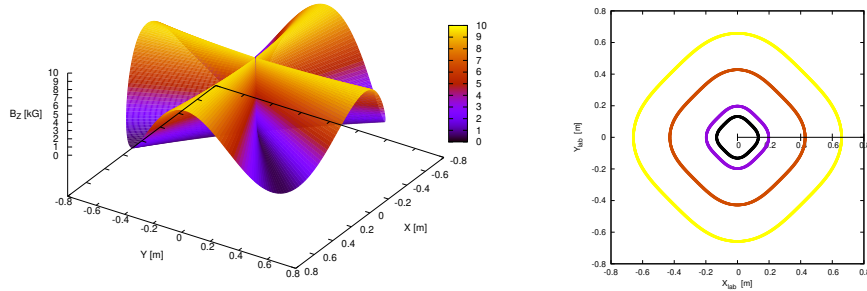


**Fig. 5.4** A 4-periodic AVF cyclotron design (after Ref. [5]). Left: mid-plane azimuthally modulated field. Right: closed orbits around the cyclotron feature azimuthally varying curvature, greater on the hills, weaker in the field valleys

by L.H. Thomas in 1938<sup>1</sup> [5] (Fig. 5.4), solved the problem: AVF results in periodic stability as long as the field modulation parameter  $F > \beta\gamma$  (Sect. 5.2.1). Spiral pole geometry was introduced in 1954 [7] for increased axial focusing, allowing greater  $k$  and isochronous acceleration to higher energy (Sect. 5.2.2). AVF cyclotrons were constructed to accelerate all sorts of ions, including polarized beams from the moment polarized ion sources were available [8], whereas classical cyclotrons gave up the land (Fig. 4.4). Applications included material science, radiobiology,

<sup>1</sup> The very L.H. Thomas of the eight years earlier Nature article on spin precession [6].

production of secondary beams. The separated sector method was developed in the early 1960s, instances are today's high power PSI 590 MeV spiral sector cyclotron (Fig. 5.2), brought into operation in 1974, and its injector-II, a radial-sector design (Fig. 5.5). Iron-free regions between separated sector dipoles allowed room for multiple high-Q RF resonators thus greater turn separation at extraction; for higher efficiency extraction systems and thus higher beam current; and for the insertion of beam instrumentation. Cyclotron energy subsequently increased, up to the present days GeV range. Cryogeny was introduced in the early 1960s at the Michigan State University K500 superconducting coil cyclotron [9] ( $K = E A/Q^2$  is a measure of the equivalent proton energy, 500 MeV in this case), allowing higher field and reduction of size, culminating today with RIKEN's K2500 SRC (Fig. 5.3).

**Fig. 5.5** PSI injector II, four separated radial sectors, 0.87 MeV injection energy, accelerates protons to 72 MeV in 100 turns. The drifts house 50.7 MHz RF systems and a flattop cavity. Injection is from the top, in the central region

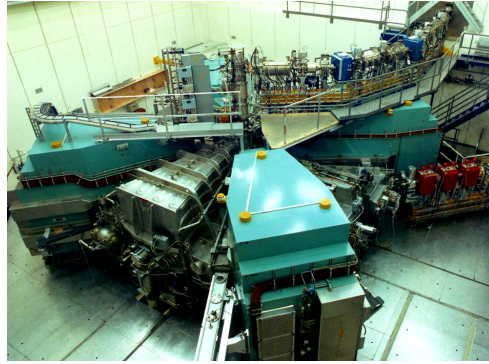


**Table 5.1** A comparison between an AVF and a separated sector cyclotron of same energy, 72 MeV, namely, the former AVF injector and the present Injector II of PSI high power cyclotron, after Ref. [8, p. 126])

		AVF	separated sector
Injection energy	keV	14	870
Extraction energy	MeV	72	72
Beam current	mA	0.2	1.6
Magnet		single dipole	4 sectors
Weight	ton	470	$4 \times 180$
Gap	mm	240 to 450	35
$\langle B \rangle$ ; $B_{\max}$	T	1.6; 2	0.36; 1.1
RF system		$180^\circ$ dees	2 resonators
Max accelerating voltage	kV	$2 \times 70$	$4 \times 250$
RF frequency	MHz	50	50
Normalized beam emittance, hor.; vert.	$\mu\text{m}$	2.4; 1.2	1.2; 1.2
Beam phase width	deg	16 - 40	12
Energy spread	%	0.3	0.2
Turn separation at extraction	mm	3	18

## 1506 5.2 Basic Concepts and Formulæ

1507 Mass increase with energy causes loss of synchronism in the classical cyclotron,  
 1508 and the required negative field index (decreasing guiding field with radius) for  
 1509 axial periodic motion stability adds to the effect. Isochronism instead, *i.e.*, constant  
 1510  $\omega_{\text{rev}} = qB/\gamma m_0$ , given orbit radius  $R = \beta c/\omega_{\text{rev}}$ , leads to positive index

$$k = \frac{R}{B} \frac{\partial B}{\partial R} = \frac{\beta}{\gamma} \frac{\partial \gamma}{\partial \beta} = \beta^2 \gamma^2 \quad (5.1)$$

1511 requiring  $k$  to follow the energy increase: the weak focusing condition  $-1 < k < 0$   
 1512 can not be satisfied, transverse periodic stability is lost.

1513 Isochronism requires the revolution period  $T_{\text{rev}} = 2\pi\gamma m_0/qB$  to be momentum  
 1514 independent; under this condition, differentiating this expression yields the radial  
 1515 field dependence

$$B(R) = \frac{B_0}{\gamma_0} \gamma(R) \quad (5.2)$$

1516 with  $B_0$  and  $\gamma_0$  some reference conditions,

1517 This led H.A. Bethe and M.E. Rose to conclude, in 1938, “... *it seems useless*  
 1518 *to build cyclotrons of larger proportions than the existing ones... an accelerating*  
 1519 *chamber of 37 cm radius will suffice to produce deuterons of 11 MeV energy which*  
 1520 *is the highest possible...*” [10]. “*If you went to graduate school in the 1940s, this*  
 1521 *inequality  $[-1 < k < 0]$  was the end of the discussion of accelerator theory.*” (Frank  
 1522 Cole [11]).

### 1523 5.2.1 Thomas Focusing

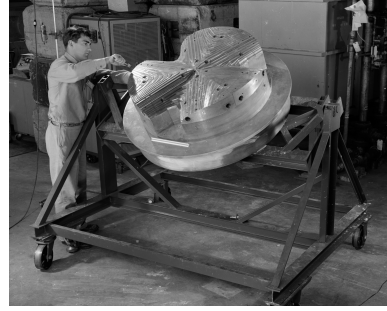
1524 Whereas the classical cyclotron approach assumed revolution symmetry of the field,  
 1525 a 1938 publication stated: “[...] *a variation of the magnetic field with angle, [...] of*  
 1526 *order of magnitude  $v/c$ ; together with nearly the radial increase of relative amount*  
 1527  *$\frac{1}{2}v^2/c^2$  of Bethe and Rose; gives stable orbits that are in resonance and not defo-*  
 1528 *cused.*” [5]. In other words, AVF in proper amount (Fig. 5.4) compensates the axial  
 1529 defocusing resulting from the increase of the field with radius (Eq. 5.2). Azimuthal  
 1530 field modulation and radial increase may be obtained by shaping the magnet poles,  
 1531 as illustrated in Fig. 5.6.

1532 *Azimuthal field modulation, flutter*

1533 A simple approach to the  $2\pi/N$ -periodic axial symmetry and field modulation may  
 1534 assume a sinusoidal azimuthal form factor

$$\mathcal{F}(\theta) = 1 + f \sin(N\theta) \quad (5.3)$$

**Fig. 5.6** Pole shaping in an AVF cyclotron, an electron model, here [12]. The focusing pattern is FfFfFf, an alternation of strong (hill regions) and weak (valleys) radial focusing [13]



As an example, this is the case in Fig. 5.4. The mid-plane field can thus be expressed under the form

$$B(R, \theta) = B_0 \mathcal{R}(R) \mathcal{F}(\theta) \quad (5.4)$$

with  $\mathcal{R}(R)$  the radial dependence of the field. The orbit curvature varies along the  $\frac{2\pi}{N}$ -periodic orbit, this requires distinguishing between the local focusing index  $n = \frac{\rho(s)}{B(s)} \frac{dB}{d\rho}$  and the geometrical index  $k$  (Eq. 5.1), a global quantity which determines the wave numbers (Eq. 5.6). A “flutter” factor can be introduced to quantify the focusing effect of the azimuthal modulation,

$$F = \left( \frac{\langle (\mathcal{F} - \langle \mathcal{F} \rangle)^2 \rangle}{\langle \mathcal{F} \rangle^2} \right)^{1/2} \xrightarrow{\text{hard edge}} \left( \frac{R}{\rho} - 1 \right)^{1/2} \quad (5.5)$$

wherein  $\langle * \rangle = \oint (*) d\theta / 2\pi$ . If the scalloping of the orbit (*i.e.*, its excursion in the vicinity of  $R$ ) is of small amplitude, then  $R \approx \rho$  and, accounting for the isochronism condition (Eq. 5.1), an approximate value of the wave numbers writes

$$\nu_R \approx \sqrt{1 + k} = \gamma, \quad \nu_y \approx \sqrt{-k + F^2} \stackrel{\text{isochr.}}{=} \sqrt{-\beta^2 \gamma^2 + F^2} \quad (5.6)$$

with the property

$$\nu_R^2 + \nu_y^2 = 1 + F^2 \xrightarrow{\text{hard edge}} \frac{R}{\rho} \quad (5.7)$$

The flutter allows designing  $-k + F^2 > 0$  (whereas  $k > 0$ ), so ensuring vertical periodic stability. In the hypothesis of a sinusoidal azimuthal field modulation (Eq. 5.3) one has  $F = f/\sqrt{2}$  and

$$\nu_y \approx \sqrt{-k + f^2/2}, \quad \nu_R^2 + \nu_y^2 = 1 + f^2/2 \quad (5.8)$$

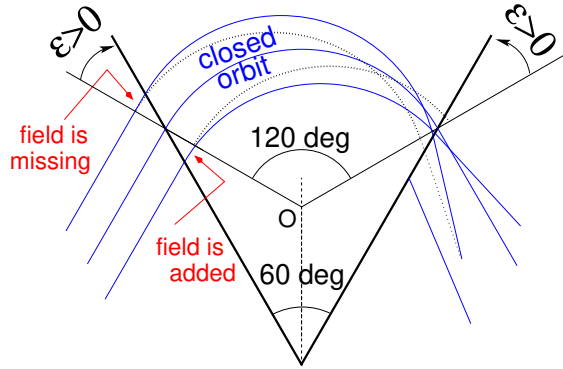
*AVF Modeling*

1550 A numerical approach to the azimuthal modulation beyond the simple sine modulation  
 1551 of Eq. 5.3, is discussed in Sect. 18.2.6 (Eqs. 18.17, 18.21). It provides a modeling  
 1552 of  $\mathcal{F}(\theta)$  over the whole beam excursion area, possibly including an R-dependence,  
 1553  $\mathcal{F}(R, \theta)$ . The method ensures the continuity of  $\mathcal{F}(R, \theta)$  and its derivatives, between  
 1554 neighboring magnetic sectors. The method is addressed further in the simulation  
 1555 exercises, where it is resorted to.

### 1556 *Wedge Focusing*

1557 In the entrance and exit regions of a bending sector, closed orbits are at an angle  
 1558 to the iso-field lines, this causes “wedge focusing”, an effect sketched in Fig. 5.7:  
 1559 with positive wedge angle  $\varepsilon$ , case of the AVF configuration, radial focusing de-  
 1560 creases whereas the angle of off mid-plane particle velocity vector to the azimuthal  
 1561 component of the field in the wedge region causes axial focusing.

**Fig. 5.7** A 120 deg bending of the closed orbit (curvature center at O) is ensured by a 60 deg bending sector. This results in a wedge angle ( $\varepsilon > 0$  by convention in this configuration) in the transition regions between valleys and hills, which causes a decrease of the radial focusing (solid incoming trajectories, compared to dotted ones), and axial focusing under the effect of the trajectory angle to the azimuthal field component



### 1562 **5.2.2 Spiral Sector**

1563 Spiral sector geometry was introduced in 1954 in the context of FFAG studies [7], and  
 1564 found application in cyclotrons (as in PSI’s COMET cyclotron, Fig. 5.1). Spiraling  
 1565 the edges (Fig. 5.8) results in stronger axial focusing (Eq. 5.11) compared to a  
 1566 radial sector (Eq. 5.6), it also permits an increase of the wedge angle with radius, so  
 1567 maintaining proper compensation of the increase of  $k(R)$  (Eq. 5.1). In a spiral sector  
 1568 bend the wedge angle is positive on one side of the sector, negative on the other  
 1569 side (Fig. 5.8), with a global vertical focusing resultant. In a similar approach to the  
 1570 periodic field modulation in a radial sector (Eq. 5.3), a convenient approach to the  
 1571 spiral sector AVF uses



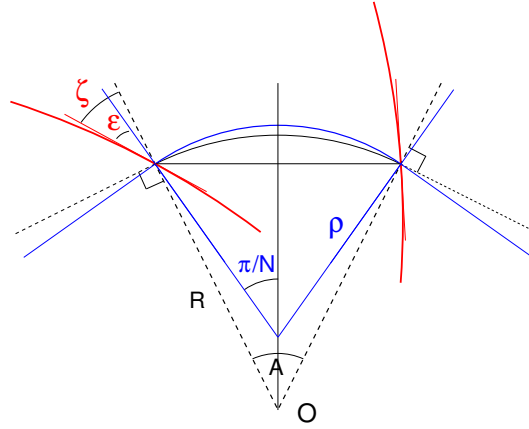
$$\mathcal{F}(R, \theta) = 1 + f \sin \left[ N \left( \theta - \tan(\zeta(R)) \ln \frac{R}{R_0} \right) \right] \quad (5.9)$$

1572 with the spiral angle  $\zeta(R)$  an increasing function of radius  $R$ , whereas the mid-plane  
1573 field is written under the form

$$B(R, \theta) = B_0 \mathcal{R}(R) \mathcal{F}(R, \theta) \quad (5.10)$$

The local magnet edge geometry at  $R$  satisfies  $r = r_0 \exp(\theta/\tan(\zeta))$ , a logarithmic

**Fig. 5.8** Geometrical parameters of a spiral sector dipole. The center of the ring is at  $O$ ,  $\zeta$  is the spiral angle (increasing with radius),  $\varepsilon$  is the wedge angle. In the hard edge field model, a line of constant field inside the sector is an arc of radius  $R$ ; thus the curvature radius  $\rho$  varies along the closed orbit in the dipole



1574 spiral centered at the center of the ring, with  $\zeta$  the angle between the tangent to the  
1575 spiral edge and the ring radius (Fig. 5.8). This results in a larger contribution of the  
1576 flutter term in the axial wave number,  
1577

$$\nu_y = \sqrt{-k + F^2(1 + 2 \tan^2 \zeta)} \quad (5.11)$$

1578 As the field index  $k$  increases with  $R$  to ensure isochronism (Eq. 5.1), the spiral angle  
1579 follows so to maintain  $-k + F^2(1 + 2 \tan^2 \zeta) > 0$ . A limitation here is the maximum  
1580 spiral angle achievable, obviously  $\zeta \rightarrow 90$  deg.

1581 As an illustration, in TRIUMF cyclotron  $\zeta$  reaches 72 deg in the 500 MeV region  
1582 (from zero in the 100 MeV region) whereas  $1 + 2 \tan^2 \zeta$  increases to 20 (from 1 in  
1583 the 100 MeV region) and compensates a low  $F < 0.07$  (down from  $F = 0.3$ ). In PSI  
1584 590 MeV cyclotron  $\zeta$  reaches 35° on the outer radius. Most isochronous cyclotrons  
1585 of a few tens of MeV use spiral sectors to benefit from the more efficient axial  
1586 focusing [13].

1587 More can be found in the scaling FFAG chapter (Sect. 11.2.2) regarding the spiral  
1588 sector, and regarding its numerical simulation.

### 1589 5.2.3 Isochronism

1590 In the hypothesis of isochronism, the revolution angular frequency satisfies  $\omega_{\text{rev}} =$   
 1591  $c\beta(\gamma)/R(\gamma) = \text{constant}$ . An orbital radius  $R_\infty = c/\omega_{\text{rev}}$  is reached asymptotically as  
 1592  $\beta = v/c = R/R_\infty \rightarrow 1$ . In terms of the RF frequency and harmonic number,

$$R_\infty = h \frac{c}{\omega_{\text{rf}}} \quad (5.12)$$

1593 Given  $BR_\infty = \gamma m_0 c/q$  and using  $\gamma = (1 - (R/R_\infty)^2)^{-1/2}$ , the radial dependence of  
 1594 the field can be expressed in terms of  $R_\infty$ , namely,

$$B_0 \mathcal{R}(R) = \gamma B_0 = \frac{B_0}{\sqrt{1 - (R/R_\infty)^2}} \quad \text{with } B_0 = \frac{m_0 \omega_{\text{rev}}}{q} = \frac{m_0}{q} \frac{\omega_{\text{rf}}}{h} \quad (5.13)$$

1595 and goes to infinity with  $R \rightarrow R_\infty$ . For protons for instance, with  $m_0/q = 1.6726 \times$   
 1596  $10^{-27}[\text{kg}] / 1.6021 \times 10^{-19}[\text{C}] \approx 10^{-8}$ ,  $BR_\infty[\text{T m}] = \gamma m_0 c/q \approx 3\gamma$ . A typical value  
 1597 for  $R_\infty$  can be obtained assuming for instance an upper  $\gamma = 1.64$  (600 MeV) in a  
 1598 region of upper field value  $B = 1.64 \text{ T}$ , yielding  $R_\infty \approx 3 \text{ m}$ .

### 1599 *Radial field*

1600 From Eq. 5.13 it results that the radial field form factor of Eqs. 5.4, 5.10 can be  
 1601 written

$$\mathcal{R}(R) = \left(1 - \left(\frac{R}{R_\infty}\right)^2\right)^{-1/2} \quad (5.14)$$

1602 A possible approach consists in using the Taylor expansion of  $\mathcal{R}(R)$  (within the limits  
 1603 of radius of convergence of that series), namely

$$\mathcal{R}(R) = 1 + \frac{1}{2} \left(\frac{R}{R_\infty}\right)^2 + \frac{3}{8} \left(\frac{R}{R_\infty}\right)^4 + \frac{5}{16} \left(\frac{R}{R_\infty}\right)^6 + \dots \quad (5.15)$$

1604 The coefficients in this polynomial in  $R/R_\infty$  are the field index and its derivatives,  
 1605 they can be a starting point for further refinement of the isochronism, including for  
 1606 instance side effects of the azimuthal field form factor  $\mathcal{F}(R, \theta)$  (Eqs. 5.3, 5.9).

1607 The radial field index  $k(R)$  in the AVF cyclotron is designed to satisfy the condition  
 1608 of isochronism (Eq. 5.1). However, reducing the RF phase slip over the acceleration  
 1609 cycle substantially below  $\pm\pi/2$  requires a tolerance below  $10^{-5}$  on field value over  
 1610 the orbit excursion area. This tight constraint requires pole machining, shimming,  
 1611 and other correction coil strategies in order to satisfy Eq. 5.1.

### 1612 *Fast Acceleration*

1613 Fixed field and fixed RF frequency allow fast acceleration, the main limitation is in  
 1614 the amount of voltage which can be implemented around the ring. The voltage per

turn reaches 4 MV for instance at the PSI 590 MeV ring cyclotron, where bunches are accelerated from 72 MeV to 590 MeV in less than 200 turns.

Harmful resonances may have to be crossed as wave numbers vary during acceleration, including the “Walkinshaw resonance”  $\nu_R = 2\nu_y$  as  $\nu_R \approx \gamma$  whereas the axial wave number takes its value in the  $\nu_y \approx 1^- \sim 1.5$  region. This coupling resonance may result in an increase of vertical beam size and subsequent particle losses, fast crossing mitigates the effect.

Fast acceleration improves extraction efficiency, as the turn separation  $dR/dn$  is proportional to the energy gain per turn (Sect. 5.2.4).

### 5.2.4 Cyclotron Extraction

The minimum radial distance between the last two turns, where the extraction septum is located, is imposed by beam loss tolerances, which in some cases (high power beams for instance) may be very tight, in the  $10^{-4}$  range or less. Space charge in particular matters, as it increases the energy spread, and thus the radial extent of a bunch. In the relativistic cyclotron the separation between two consecutive turns satisfies

$$\Delta R \approx \frac{\gamma}{\gamma + 1} \frac{\Delta E}{E} \frac{R}{\nu_R^2} \quad (5.16)$$

with  $\Delta E$  the effective acceleration rate per turn. Referring to Eq. 5.12, it indicates that a greater RF harmonic allows greater extraction radius and benefits extraction efficiency; it results from Eq. 5.16 that a large ring is an additional option for greater turn separation at extraction, and as a matter of fact size is a limitation to intensity in small cyclotrons.

In low energy cyclotrons ( $\gamma$  close to 1), extraction efficiency may also be increased by moving the wave number  $\nu_R \approx \gamma$  close to the integer resonance  $\nu_R = 1$ .

### 5.2.5 Resonant Spin Motion

In the quasi-uniform, quasi vertical field  $\mathbf{B} \approx \mathbf{B}_y$  of a classical cyclotron dipole, spins quietly perform  $G\gamma$  precessions around a vector  $\omega_{sp} \parallel \mathbf{B}$  (Eq. 4.28) as the particle velocity completes a  $2\pi$  precession around the ring (Sect. 4.2.5) [15].

More is liable to happen in the AVF cyclotron, due to the strong radial field index (Eq. 5.1) and to the azimuthal field modulation (Eqs. 5.3, 5.9): the azimuthal and radial field components  $B_\theta$  and  $B_R$  are non-zero out of the median plane,  $\mathbf{B}(R, \theta, y)$  may locally depart from the vertical in a substantial manner, and so will the local precession vector  $\omega_{sp}(R, \theta, y)$ . The latter varies periodically in addition, as the particle undergoes a vertical periodic motion about the median plane. Resonance between spin precession (characterized by spin tune  $\nu_{sp} = G\gamma$ , Eq. 4.31) and periodic perturbing field components (characterized by the vertical wave number  $\nu_y$ , Eqs. 5.6, 5.11)

occurs if the two motions feature coinciding frequencies. This condition can be expressed under the form

$$\nu_{\text{sp}} \pm \nu_y = \text{integer} \quad \text{or, equivalently} \quad G\gamma = \text{integer} \pm \nu_y \quad (5.17)$$

The spin precession axis  $\omega_{\text{sp}}$  moves away from the vertical as the spin motion gets closer to resonance (during acceleration as  $G\gamma$  varies for instance), to end up in the median plane on the resonance.

Consider now an ion bunch, away from any depolarizing resonance. Its polarization is  $\langle S_y \rangle$ , the average of the projection of the spins on the vertical. If a depolarizing resonance is crossed during acceleration, the initial polarization (far upstream of the resonance; index i) and final polarization (far downstream of the resonance; index f) satisfy the Froissart-Stora law [16],

$$\frac{\langle S_y \rangle_f}{\langle S_y \rangle_i} = 2e^{-\frac{\pi}{2} \frac{|\epsilon_R|^2}{a}} - 1 \quad (5.18)$$

wherein  $|\epsilon_R|$  is the strength of the resonance: a measure of the strength of the depolarizing fields, its calculation is addressed in a next chapter;  $a$  is the resonance crossing speed,

$$a = G \frac{d\gamma}{d\theta} \pm \frac{d\nu_y}{d\theta} \quad (5.19)$$

The Froissart-Stora formula indicates that, if the resonance is crossed slowly ( $a \rightarrow 0$ ),  $\langle S_y \rangle_f / \langle S_y \rangle_i \rightarrow -1$ : spins follow the flipping motion of the precession axis, polarization is flipped and preserved. If the crossing is fast ( $a \rightarrow \infty$ ),  $\langle S_y \rangle_f / \langle S_y \rangle_i \rightarrow 0$ , polarization is unaffected. Intermediate crossing speeds cause polarization loss:  $|\langle S_y \rangle|$  ends up smaller after the resonance.

## 5.3 Exercises

Exercises 5.2 to 5.4 use a field map, designed in exercise 5.1, to simulate an AVF cyclotron dipole. Note that they can be performed using DIPOLE[S] analytical field model instead, as in exercise 5.5 (a similar simulation which can be referred to is exercise 4.2, Classical Cyclotron Chapter). As a reminder, regarding the interest of one or the other of the two methods: field maps allow close to real field models (a measured field map for instance, or from a magnet computer code); using an analytical field model allows more flexibility regarding magnet parameters, which can for instance be optimized using a matching procedure.

### 5.1 Modeling Thomas AVF Cyclotron

Solution: page 310.

In this exercise a 2D mid-plane field map is built, inspired from Thomas's 1938 article [5]. The method to build the map is that of Exercise 4.1, TOSCA keyword is used to raytrace through and derive the optical parameters of the 4-period AVF cyclotron.

(a) Construct a  $360^\circ$  2D map of the median plane field  $B_Z(R, \theta)$ , simulating the field in the 4-period Thomas cyclotron of Fig. 5.4, assuming the following:

- $B_Z(R, \theta) = B_0[1 + f \sin(4(\theta - \theta_i))]$  (Eq. 5.3), with  $\theta_i$  some arbitrary origin of the azimuthal angle, to be determined. Hint: depending on  $\theta_i$  value, the closed orbit may be at an angle to the polar radius, as seen in Fig. 5.4; in that case TOSCA would require non-zero in and out positioning angles TE and TS, to be determined and stated using KPOS option [17]; instead, a proper choice of  $\theta_i$  value allows a simpler TE=TS=0;

- an average axial field  $B_0 = 0.5$  T on the 200 keV radius (the latter,  $R_0(B_0)$ , is to be determined),  $B_Z > 0$  and  $0 < f < 1$  modulation.

- an arbitrary field index  $k$  - a good idea is to start building and testing the AVF in the case  $k = 0$ ;

- a uniform map mesh in a polar coordinate system  $(R, \theta)$  as sketched in Fig. 4.17, covering  $R=1$  to 100 cm; take a radial increment of the mesh  $\Delta R = 0.5$  cm, azimuthal increment  $\Delta\theta = 0.5 \text{ cm}/R_M$ , with  $R_M$  some reference radius, say  $R_M = 50$  cm, half way between map boundaries;

- an appropriate 6-column formatting of the field map data for TOSCA to read, as follows:

$$R \cos \theta, Z, R \sin \theta, BY, BZ, BX$$

with  $\theta$  varying first,  $R$  varying second in that list. Z is the vertical direction (normal to the map mesh), so  $Z \equiv 0$  in this 2D mesh.

Provide a graph of  $B_Z(R, \theta)$  over the extent of the field map.

(b) Raytrace a few concentric closed trajectories centered on the center of the dipole, ranging in  $10 \leq R \leq 80$  cm. Provide a graph of these concentric trajectories in the  $(O; X, Y)$  laboratory frame, and a graph of the field along trajectories. Initial coordinates can be defined using OBJET, particle coordinates along trajectories during the stepwise raytracing can be logged in zgoubi.plt by setting IL=2 under TOSCA.

(c) Check the effect of the integration step size on the accuracy of the trajectory and time-of-flight computation, by considering some  $\Delta s$  values in  $[0.1, 10]$  cm, and energies in a range from 200 keV to a few tens of MeV (considering protons).

(d) Produce a graph of the energy or radius dependence of wave numbers.

(e) Calculate the numerical value of the axial wave number,  $\nu_y$ , from the flutter (Eqs. 5.5, 5.6). Comparing with the numerical values, discrepancy is found: repeat (d) for  $f=0.1, 0.2, 0.3, 0.6$ , check the evolution of this discrepancy.

## 5.2 Designing an Isochronous AVF Cyclotron

Solution: page 319.

(a) Introduce a radius dependent field index  $k(R)$  in the AVF cyclotron designed in exercise 5.1, proper to ensure R-independent revolution period, in three different cases of modulation:  $f=0$  (no modulation),  $f=0.2$  and  $f=0.9$ .

Check this property by computing the revolution period  $T_{\text{rev}}$  as a function of kinetic energy  $E_k$ , or radius  $R$ . On a common graph, display both  $T_{\text{rev}}$  and  $dT_{\text{rev}}/T_{\text{rev}}$  as a function of radius, including for comparison a fourth case:  $B=\text{constant}=5$  kG.

(b) Provide a graph of the energy dependence of wave numbers.

## 5.3 Acceleration to 200 MeV in an AVF Cyclotron

Solution: page 325.

In this exercise protons are accelerated to over 100 MeV in an AVF cyclotron: well beyond the about 20 MeV energy reached in the classical cyclotron (see exercise 4.10).

(a) Produce an acceleration cycle of a proton, from 0.2 to 100 MeV, in the AVF cyclotron designed in exercise 5.2. Note that a dedicated field map has to be created in order to allow for the higher maximum energy - a 3 meter field map outer radius works. Assume proper modulation coefficient  $f$  for axial focusing all the way to 300 MeV. Assume a double-dee design, and 400 keV peak voltage in the gap, use CAVITE[IOPT=7] for acceleration to account for RF phase.

(b) Give a graph of the energy dependence of wave numbers over the acceleration range.

## 5.4 Thomas-BMT Spin Precession in Thomas Cyclotron

Solution: page 328.

This exercise uses the field maps and input data file of exercise 5.3. Dependence of energy boost on RF phase is removed by using CAVITE[IOPT=3] [17]. Consider helion ions: use PARTICUL[Name=HELION] to define mass, charge and G factor, all quantities needed for the integration of Thomas-BMT differential equation (Eq. 4.28).

(a) By scanning the vertical wave number, find the  $G\gamma$  value for which the spin motion resonance condition (Eq. 5.17) is satisfied.

(b) Consider a particle with non-zero axial motion, so that it experiences horizontal magnetic field components as it cycles around. Track its spin through the resonance, take initial spin vertical  $\mathbf{S} \equiv \mathbf{S}_Z$ . Provide a graph of  $S_Z$  as a function of  $G\gamma$  or energy.

(c) Simulate resonance crossings for a series of different vertical motion amplitudes  $Z_0$ ; produce a graph of these resonance crossings  $S_Z(turn)$ .

Plot the ratio  $S_{y,f}/S_{y,i}(Z_0)$ . From a match of this  $S_{y,f}/S_{y,i}$  series with Eq. 5.18, show that the resonance strength changes in proportion to the vertical excursion.

(d) Repeat (c) for a series of different resonance crossing speeds instead (Eq. 5.19), leaving  $Z_0$  unchanged.

Show that this  $S_{y,f}/S_{y,i}$  series can be matched with Eq. 5.18.

## 5.5 Isochronism and Edge Focusing in a Separated Sector Cyclotron

Solution: page 332.

This exercise uses DIPOLE to simulate a 30 deg sector dipole of a 4-period cyclotron, and allow playing with field fall-off extent at dipole EFBs. The configuration of the cyclotron is typically that of PSI 72 MeV injector (Fig. 5.5). DIPOLE allows radial field indices up to the third order ( $\partial^3 B_Z / \partial R^3$ ) [17, Eq. 6.3.18]. In question (b) however, higher order indices are needed to improve the isochronism, requiring the use of DIPOLES [17, Eqs. 6.3.20, 21].

Take fringe fields into account (see Sect. 18.2.6), with

- $\lambda = 7$  cm the fringe extent (changing  $\lambda$  changes the flutter, Eq. 5.5),
- $C_0 = 0.1455$ ,  $C_1 = 2.2670$ ,  $C_2 = -0.6395$ ,  $C_3 = 1.1558$  and  $C_4 = C_5 = 0$ , for a realistic field fall-off model.

(a) Assume  $k = 0$ , here. Produce a model of a period using DIPOLE.

Produce a graph of closed orbits across a period for a few different rigidities (FIT can be used to find them), and a graph of the field along these orbits.

(b) In this question, R-dependence of the mid-plane magnetic field proper to ensuring energy independent revolution period is introduced. Use DIPOLES here, as it allows  $b_i$  field indices to higher order, as necessary to reach tight isochronism over the full energy range.

Assume a peak field value  $B_0 = 1.1$  T at a radius of 3.5 m in the dipoles. Find the average orbit radius  $R$ , and average field  $B$  (such that  $BR = p/q$ ), at an energy of 72 MeV.

Determine a series of index values,  $b_{i=1,n}$ , in the model [17, Eq. 6.3.19]

$$B_Z(R, \theta) = B_0 \mathcal{F}(R, \theta) \left( 1 + b_1 \frac{R - R_0}{R_0} + b_2 \left( \frac{R - R_0}{R_0} \right)^2 + \dots \right) \quad (5.20)$$

proper to bring the revolution period closest to R-independent, in the energy range 0.9 to 72 MeV (hint: use a Taylor development of Eq. 5.14 and identify with the R-dependent factors in Eq. 5.20).

(c) Play with the value of  $\lambda$ , concurrently to maintaining isochronism with appropriate  $b_i$  values. Check the evolution of radial and axial focusing - OBJET[KOBJ=5] and MATRIX can be used to get the wave numbers.

From raytracing trials, observe that (i) the effect of  $\lambda$  on radial focusing is weak (a second order effect in the particle coordinates); (ii) greater (smaller)  $\lambda$  value results in smaller (greater) flutter and weaker (stronger) axial focusing (a first order effect). Note: the integration step size in DIPOLE[S] has to be consistent with the value

1793 field fall-off extent ( $\lambda$  value), in order to ensure that the numerical integration is  
 1794 converged.

1795 (d) For some reasonable value of  $\lambda$  (normally, about the height of a magnet  
 1796 gap, say, a few centimeters), compute  $F^2 = \left\langle \left( \frac{B(\theta) - \langle B \rangle}{\langle B \rangle} \right)^2 \right\rangle$ . Check the validity of  
 1797  $\nu_y = -\beta^2 \gamma^2 + F^2$  (Eq. 5.6). MATRIX can be used to compute  $\nu_y$ , or multiturn  
 1798 raytracing and a Fourier analysis.

1799 (e) Check the rule  $F^2 \xrightarrow{\text{hard edge}} \frac{R}{\rho} - 1$  (Eq. 5.5), from the field  $B(\theta)$  delivered by  
 1800 DIPOLES. Give a theoretical demonstration of that rule.

## 1801 5.6 A Model of PSI Ring Cyclotron Using CYCLOTRON

1802 Solution: page 335.

1803 The simulation input data file in Tab. 5.2 is based on the use of CYCLOTRON, to  
 1804 simulate a period of the eight-sector PSI ring cyclotron and work on the isochronism.  
 1805 That file is the starting point of the present exercise.

1806 (a) With zgoubi users' guide at hand, explain the signification of the data in that  
 1807 simulation input data file.

1808 (b) Compute and plot a few trajectories and field along, across the sector. Provide  
 1809 a graph of field density over the sector.

1810 (c) Compute and plot the radius dependence of the revolution period.

1811 (d) The field indices  $b_1, b_2, \dots$  are aimed at realizing the isochronism; four,  $b_1 - b_4$   
 1812 are accounted for in (a) and (b), they were drawn from the PSI cyclotron spiral sector  
 1813 magnet field map data. Question (c) proves this small set of indices to result in a  
 1814 poor isochronism of the orbits.

1815 Add higher order indices, until a sufficient number, with proper values, is found  
 1816 that allows FIT to reach a final isochronism improved by an order of magnitude.  
 1817 Provide a revised input data file with updated index series and their values.



**Table 5.2** Simulation input data file: a period of an eight-sector PSI-style cyclotron. The data file is set up for a scan of the periodic orbits, from radius  $R=204.1171097$  cm to  $R=383.7131468$  cm, in 15 steps

```

PSI CYCLOTRON

'OBJET'
1249.382414
2
1 1
204.1171097 8.915858372 0. 0. 0. 1. 'o'
1
'PARTICUL'
PROTON

'CYCLOTRON'
2
1 45.0 276. 1.0
0. 0. 0.99212277 51.4590015 0.5 800. -0.476376328 2.27602517e-03 -4.8195589e-06 3.94715806e-09
18.3000E+00 1. 28. -2.0
8 1.1024358 3.1291507 -3.14287154 3.0858059 -1.43545 0.24047436 0. 0. 0.
11.0 3.5 35.E-3 0.E-4 3.E-8 0. 0. 0.
18.3000E+00 1. 28. -2.0
8 0.70490173 4.1601305 -4.3309575 3.540416 -1.3472703 0.18261076 0. 0. 0.
-8.5 2. 12.E-3 75.E-6 0. 0. 0. 0.
0. -1
0 0. 0. 0. 0. 0. 0. 0.
0. 0. 0. 0. 0. 0.
2 10.
0.4
2 0. 0. 0. 0.

'FIT2'
2
1 31 0 [-300.,100]
1 35 0 [.1,3.]
2
3.1 1 2 #End 0. 1. 0
3.1 1 3 #End 0. 1. 0
'FAISCEAU'

'FAISTORE'
orbits.fai
1

'REBELOTE'
14 0.2 0 1
1
OBJET 30 221.065356:383.7131468

'SYSTEM'
1
gnuplot <./gnuplot_orbits.gnu
'END'

```

## References

1. J.M. Schippers, J.M.: The Superconducting Cyclotron and Beam Lines of PSI's New Proton Therapy Facility "PROSCAN". 17th International Conference on Cyclotrons and their Applications: Tokyo, Japan; 18-22 October 2004.  
[http://accelconf.web.cern.ch/c04/data/CYC2004\\_papers/20B2.pdf](http://accelconf.web.cern.ch/c04/data/CYC2004_papers/20B2.pdf). Copyrights under license CC-BY-3.0, <https://creativecommons.org/licenses/by/3.0/>; no change to the material
2. Seidel, M.: Production of a 1.3 Megawatt Proton Beam at PSI. Proceedings of IPAC'10, Kyoto, Japan, TUYRA03.  
[http://accelconf.web.cern.ch/IPAC10/talks/tuyra03\\_talk.pdf](http://accelconf.web.cern.ch/IPAC10/talks/tuyra03_talk.pdf). Copyrights under license CC-BY-3.0, <https://creativecommons.org/licenses/by/3.0/>; no change to the material
3. Kawaguchi, T., et al., Design of the sector magnets for the RIKEN superconducting ring cyclotron, Proceedings of the 15th International Conference on Cyclotrons and their Applications, Caen, France.  
<https://accelconf.web.cern.ch/c98/papers/b-14.pdf>  
 Fig. 5.3: the picture, and the permission to use it in this publication, has been provided by RIKEN (January 2023)
4. <http://accelconf.web.cern.ch/c07/OTHERS/Cyclotron%20List%202007%20-Full.pdf>
5. Thomas, L.H.: The Paths of Ions in the Cyclotron. Phys. Rev. 54, 580, (1938)
6. Thomas, L.H.: Motion of the spinning electron. Nature. 117 (2945): 514 (1926)
7. Symon, K.R., et al.: Fixed-Field Alternating-Gradient Particle Accelerators. Phys. Rev. 103, 1837 (1956)
8. Stambach, T.: Introduction to Cyclotrons. CERN accelerator school, cyclotrons, linacs and their applications, IBM International Education Centre, La Hulpe, Belgium, 28 April-5 May 1994. Copyright/License CERN CC-BY-3.0 - <https://creativecommons.org/licenses/by/3.0/>
9. Miller, P.S., et al.: The Magnetic Field of the K500 Cyclotron at MSU Including Trim Coils and Extraction Channels. Procs. 9th Int. Conf. on Cyclotrons and their Applications, September 1981, Caen, France.  
<http://accelconf.web.cern.ch/c81/papers/ep-05.pdf>
10. Bethe, H.A. and Rose, M.E., Phys. Rev. 54, 588 (1938)
11. After Baartman, Rick: Cyclotrons, Classic to FFAG. FFAG Workshop \*\*\*\*\* to be completed \*\*\*\*\*.
12. © The Regents of the University of California, Lawrence Berkeley National Laboratory
13. Craddock, M.K.: AG focusing in the Thomas cyclotron of 1938, Proceedings of PAC09, Vancouver, BC, Canada, FR5REP1.  
<http://accelconf.web.cern.ch/PAC2009/papers/fr5rep113.pdf>
14. Joho, W.: The Cyclotron Facilities at PSI. Seminar slides, PSI, 2013 (unpublished)
15. Méot, F.: Spin Dynamics. Polarized Beam Dynamics and Instrumentation in Particle Accelerators: USPAS Summer 2021 Spin Class Lectures, Springer (2023)
16. Froissart, M., Stora, R.: Depolarisation d'un faisceau de protons polarisés dans un synchrotron. Nuclear Instruments and Methods. 7 (3): 297-305 (June 1960)
17. Méot, F.: Zgoubi Users' Guide.  
<https://www.osti.gov/biblio/1062013-zgoubi-users-guide> Sourceforge latest version:  
<https://sourceforge.net/p/zgoubi/code/HEAD/tree/trunk/guide/Zgoubi.pdf>